Computational Investigation into Predicting Total Resistance of Axe-Bow Ship's in Calm Water

Ahmad Fitriadhy[1,*], Rizuan Razali[2], Atiqah Yaakup[2], M. Ridwan Utina[3], Anuar Abu Bakar[1], Alamsyah Kurniawan[4], Budianto Ontowirjo[5]

[1] Program of Naval Architecture, Faculty of Ocean Engineering Technology and Informatics, Universiti Malaysia Terengganu, Kuala Terengganu, Terengganu, Malaysia
[2] Postgraduate Student, Faculty of Ocean Engineering Technology and Informatics, Universiti Malaysia Terengganu, Kuala Terengganu, Terengganu, Malaysia
[3] Research Center for Hydrodynamics Technology, The National Research and Innovation Agency (BRIN), Indonesia
[4] Coastal Engineering Research, Faculty of Civil and Environmental Engineering, Institut Teknologi Bandung, Indonesia
[5] Civil Engineering Department, Bakrie University, Jakarta, Indonesia

ARTICLE INFO	ABSTRACT
                 	The axe-bow ship design has been primarily introduced to minimize ship's slamming condition during sailing, which inherently deals with sufficient of her total ship's resistance. The presence of nonlinear-hydrodynamic flow behaviours around the ship will forcefully impose pressure and viscous resistances on her hull. This complex phenomenon is so intricate that a reliable approach leading into more feasible prediction of her total ship's resistance (R_T) is necessarily required, while explaining the rationale behind the analysis results. This paper presents a computational investigation into prediction total ship's resistance of an axe-bow hull in the calm water condition. Here, the Computational Fluid Dynamic (CFD) software called Numeca Fine Marine was accordingly used. Several parameters such as various Froude numbers (Fr) and trim's angles, have been taken into account in the computational simulations. The results showed that the viscous ship's resistance has more relatively significant influence on the axe-bow ship than the pressure ship's resistance especially at Fr ≥ 0.568. It is noteworthy that this causes the pressure resistance coefficient (C_P) decrease indicated with moderately diminished high-pressures acting on the axe-bow ship's hull. The increase of the trim's angle demonstrates that the existence of the higher turbulent viscosity extends over the entire submerged hull surfaces and causes reduction of the viscous coefficient (C_V). In general, the subsequent increase of Froude number and the trim's angle were proportionally to the total ship's resistance. It can be concluded that the current computational results are useful as preliminary prediction of the total ship's resistance towards determining the effective power.

1. Introduction

For the last few decades, marine transportation has heavily used in marine industry. The phenomena of a ship's slamming or known as the impact of ship's bottom structure on the water

---

* Corresponding author.
E-mail address: a.fitriadhy@umt.edu.my (Ahmad Fitriadhy)

surface during sailing at the sea may result into the increase of the total ship's resistance. This occurs since the bow part of the ship oscillates excessively in the waves, which is proportional with the increase of the pressure resistances. To resolve this problem, the Ulstein Group has proposed axe-bow design model. The Ulstein axe-bow is dominated by a high and rounded, which expands slightly at top of the ship's bow, where this feature is suitable model to increase comfortability of the passenger on-board particularly in the harsh conditions [1]. Merely, the ship leads to have better seakeeping performance presented in the form of less vertical notion in the head-sea condition. Inherently, it leads to reduce sufficiently the ship's vibrations as well as her total ship's resistance. Therefore, an investigation into predicting the total resistance of the axe-bow ship aimed at gaining better understanding of her resistance behaviour is primarily required.

Several researchers have extensively studied the axe-bow ships to predict the total ship's resistance both of using theoretical and experimental approaches. Mosaad *et al.,* [2] stated that at low Froude numbers, the wave-making resistance is reduced in the model with the axe-bow. It is noted that the wave-making resistance reduced by 29% at the low Froude numbers; whilst this decreased by 14% at the intermediate Froude number and subsequently dropped by 6% as the speed further increased. Similarly, Basil and Waris [3] found that the optimum Ulstein axe-bow's design reduced the ship's total resistance by 4% and 11% at the operational and the trawling speeds, respectively. The use of the axe-bow hull form for fishing trawlers was discovered to be a highly promising advancement over the current hull forms in terms of resistance and fuel efficiency. Simanjuntak *et al.,* [4] employed Ulstein axe-bow model on Pioneer ship 750 DWT and obtained the total ship's resistance decreased by 4.85% in the deep-water condition with h/t=19.3. Furthermore, Chen *et al.,* [5] reported that the added ship's resistance in the waves condition with the axe-bow is smaller than the wave-piercing bow at the same forward speed. In particular, the investigation on predicting the total ship's resistance using the experimental model test for the validation purposes of numerical models is much recommended. However, this physical model test was proven to be very impractical, costly and time-consuming [6-8]. Nevertheless, a more sophisticated approach to address the limitations of the conventional numerical simulation methods, a more reliable approach is still encouraged. Therefore, the Computational Fluid Dynamics approach has taken place as the feasible approach to predict the ship's resistance especially in the preliminary design stage as previously conducted by Fitriadhy *et al.,* [9,11-13], Fitriadhy and Adam [10]. The rapid increasing capabilities of computers allows to take a fully hydrodynamic approach to the fluid-body interaction problem; so that more precise solution with reasonable accuracy can be optimistically achieved.

This paper presents a computational investigation into predicting total resistance of axe-bow ship in the calm water condition. Here, commercial Computational Fluid Dynamic (CFD) software, namely NUMECA Fine Marine, is utilized by applying the incompressible unsteady Reynolds Averaged Navier Stokes Equation (RANSE). This RANSE and continuity equations are discretized by the finite volume method based on Volume of Fluid (VOF) to deal with the non-linear free surface. In addition, the computational domain with adequate numbers of grid meshes of the axe-bow ship has been accordingly set-up. Basically, this is solved by means of a mesh independent study to estimate the optimum meshing discretization. Several parameters such as various Froude numbers (Fr) with the range of 0.39460≤Fr≤0.74397 and trim's angles have been taken into account in this computational simulation. The results are clearly discussed with respect to the total ship's resistance characteristics, which are quantified by the magnitude of the pressure and viscous resistances.

2. Methodology

2.1 Governing Equation

The Navier-Stokes equation (RANSE) and the Volume of Fluid (VOF) approach for simulating free surface flow, which essentially incorporates continuity and momentum equations, are the major equations used by CFD on a regular basis. The current CFD simulation is based on the incompressible unsteady RANSE, which solves a free surface model using VOF.

2.1.1 Conservation equations

ISIS-CFD was used to solve the unsteady RANSE in a multi-phase continuum in this work. The continuity and momentum equations are simplified because the flow is deemed incompressible, but the energy equation is no longer used [11,14]. The mass and momentum conservation equations can be represented as follows when considering incompressible viscous fluid flow under isothermal conditions:

$$\frac{\partial}{\partial t}\int_v \rho dV + \int_s \rho(v\vec{U} - \vec{U}_a).\vec{\eta}dS = 0 \tag{1}$$

$$\frac{\partial}{\partial t}\int_v \rho U_i dV + \int_s \rho U_i(\vec{U} - \vec{U}_a).\vec{\eta}dS = \int_s (\tau_{ij}l_j - pl_i).\vec{n}.dS + \int_v pg_i dv \tag{2}$$

where V is the control volume bounded by the closed surface S with a unit normal vector $\vec{\eta}$ that moves at the velocity $\vec{U}_a$ While $\vec{U}$ and ρ represent the velocity and pressure field, respectively. Then, l is the identity matrix, τ_{ij} represents the viscous stress tensor components and g_i as the gravity vector. The Volume of Fluid (VOF) is applied to build the spatial discretization of the transport equations. The viscous free-surface flow is captured using the VOF approach (interface capturing techniques) where requires another solution of transport equation to determine the proportion of fluid in each cell.

2.1.2 Turbulence model

The SST $\kappa - \omega$ (SST for shear-stress transport) model in the present CFD simulation, which is available inside the ISIS-CFD solver code, where κ is the turbulent kinetic energy and ω is the particular dissipation rate. The SST $\kappa - \omega$ model, according to Menter and Rumsey [15], incorporates several desirable characteristics of existing two-equation models. The SST $\kappa - \omega$ model is used to improve the predictions achieved with algebraic mixing-length models, construct a local model for complex flows, and provide a simpler alternative for two-equation turbulence models, according to Spalart and Allmaras [16]. The model's two transport equations are defined below, with a blending function ω for the original, ε model equations, F_1 model coefficients and written as:

$$\frac{\partial \rho K}{\partial t} + \frac{\partial}{\partial x_j}\left(\rho U_j K - (\mu + \sigma_K \mu_t)\frac{\partial K}{\partial X_j}\right) = \tau_{ij}s_{ij} - \beta^*\rho\omega K \tag{3}$$

$$\frac{\partial \rho \omega}{\partial t} + \frac{\partial}{\partial x_j}\left(\rho U_j \omega - (\mu + \sigma_\omega \mu_t)\frac{\partial \omega}{\partial X_j}\right) = P_\omega - \beta\rho\omega^2 + 2(1 - F_1)\frac{\rho\sigma_{\omega 2}}{\omega}\frac{\partial K}{\partial x_j}\frac{\partial \omega}{\partial x_j} \tag{4}$$

where the cross-diffusion term appears in the transformed ω - equation from the original ω-equation, and the last source term of Eq. (6) represents it. The production term of is sometimes approximated as proportionate to the absolute value vorticity, according to Menter and Rumsey [15].

$$P_\omega = 2\gamma\rho \left(S_{ij} - \frac{\omega S_{nn}\delta_{ij}}{3} \right) S_{ij} \cong \gamma\rho\Omega^2 \tag{5}$$

The auxiliary blending function F_1, designed to blend the model coefficient of the original $\kappa - \omega$ model in boundary layer zones with the transformed $\kappa - \varepsilon$ model in free-shear layer and free-stream zones, is defined as follows:

$$F_1 = \{[\min \{\max\{\frac{\sqrt{k}}{0.09K\omega'}, \frac{500\mu}{\rho d^2\omega}\}, \frac{4\emptyset\sigma_{\omega 2}K}{CD_{k\omega}d^2}\}]^4\} \tag{6}$$

where $CD_{k\omega} = max\{\frac{2\rho\sigma_2}{\omega}\frac{\partial K}{\partial X_j}\frac{\partial\omega}{\partial X_j}, 10^{-20}\}$. Here $CD_{k\omega}$ is the cross-diffusion in the $\kappa - \omega$ model.

2.1.3 Ship resistance

ISIS-CFD According to resistance theory, a ship's total resistance can be described as the sum of frictional resistance (R_F) and pressure resistance (R_p) in Eq. (8).

$$R_T = R_P + R_V \tag{7}$$

Here the coefficient of the total resistance is expressed as [17]:

$$C_T = \frac{R_T}{0.5 \, x \, \rho \, x \, WSA \, x \, V_s{}^2} \tag{8}$$

where, R_T is the dimensional total resistance, ρ is the water density, WSA is the wetted surface area of the ship at rest and V_s is the forward speed.

2.2 Simulation Condition
2.2.1 Principal data of ship

The body plan of the axe-bow ship is clearly displayed in Figure 1. The principal dimension of the axe-bow ship is completely presented in Table 1. In the current computational simulation, several parameters such as the effect of Froude numbers and trim angles have been taken into consideration (see Table 2).
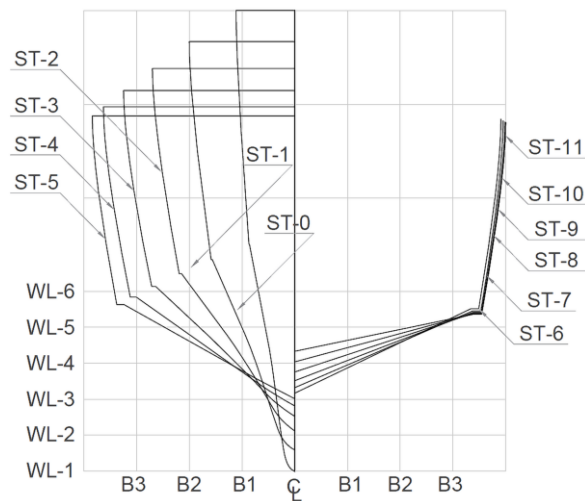
Fig. 1. Body Plan of Axe-Bow Ship

Table 1
Principal Dimensions of Axe-Bow Ship

Geometrical Parameter	Full Scale	Model Scale
Length Overall, LOA (m)	56.690	4.049
Length Between perpendicular, LBP (m)	56.366	3.867
Beam, B (m)	15.757	1.125
Draft, T (m)	7.589	0.542

Table 2
Parametric Studies

α (º)	Froude Number								
	0.396	0.437	0.481	0.525	0.568	0.611	0.655	0.700	0.744
0	√	√	√	√	√	√	√	√	√
1	-	-	-	-	-	-	-	-	√
2	-	-	-	-	-	-	-	-	√

2.2.2 Computational domain and meshing generation

The computational domain and boundary condition of the axe-bow ship model associated with the unstructured hexahedral meshes is shown in Figure 2. The dimensions of the domains for this CFD simulation are presented in Table 3. The authors used the symmetrical computational domain model to shorten the computation time (for all simulation conditions). The additional local mesh has been added into the axe-bow geometry to purposely refine her meshing quality. Correspondingly, the number of local meshing refinements of the ship's geometry is set to the maximum global number of refinements. Meanwhile, another surface is employed as a triangle purposed to capture the effective area in both x and y directions, where the Kelvin waves will appear. The symmetrical half model of the axe-bow model has been applied in the computational domain for dealing with less computational time.
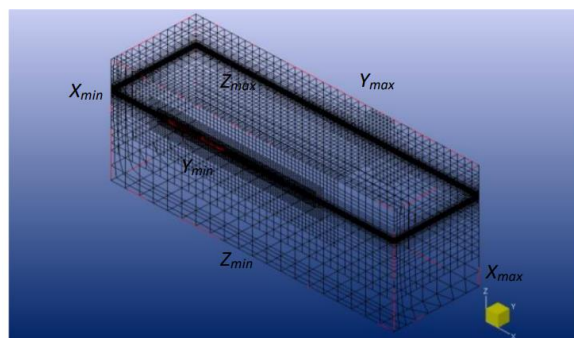
Fig. 2. Mesh generation of Axe-Bow Ship

Table 3
Computational Domain and Boundary Setting Conditions

Description	Distance From COG	Type	Condition
X_{min} (Inlet)	1.0 L	EXT	Far Field
X_{max} (Outlet)	3.0 L	EXT	Far Field
Y_{min} (Side)	1.5 L	MIR	Mirror
Y_{max} (Side)	1.5 L	EXT	Far Field
Z_{min} (Bottom)	1.5 L	EXT	Prescribed Pressure
Z_{max} (Top)	0.5 L	EXT	Prescribed Pressure

The boundary condition of the computational simulation has accordingly been assigned as summarized in Table 3. The external (EXT) boundary type condition is attributed to treat either velocity or pressure conditions. Furthermore, the vertical boundary conditions both of the top and bottom of the patch's domain are specified as 'prescribed pressure'. In this mode, the pressure is initially imposed in the computational simulation to dynamically produce the updated hydrostatics pressure. This identify that the hydrostatics pressure is not constant 0 (zero), but it dynamically updates since the cell mesh moves vertically towards the free surface elevation. In addition, the axe-bow ship surfaces are defined as solid patches, where a wall-function condition was applied to the model surfaces. Figure 3 shows the time History on Axe-Bow Ship.
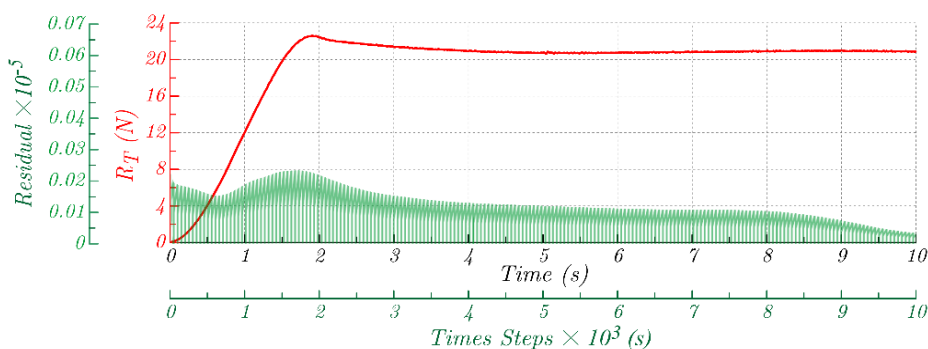
Fig. 3. Time History on Axe-Bow Ship's at Trim Angle = 0° and Fr = 0.655

3. Results

The computational investigation into the predicting the total ship's resistance in the calm water condition has primarily involved two parameters i.e., the Froude numbers and the trim's angle as clearly written above. The findings have been appropriately discussed with respect to the total ship's resistance, which is basically composed into the pressure and viscous ship's resistances. The details

of the computational results are presented in Sub-sections 3.1 and 3.2, respectively. Figure 4 shows the Visualization on Axe-Bow Ship.
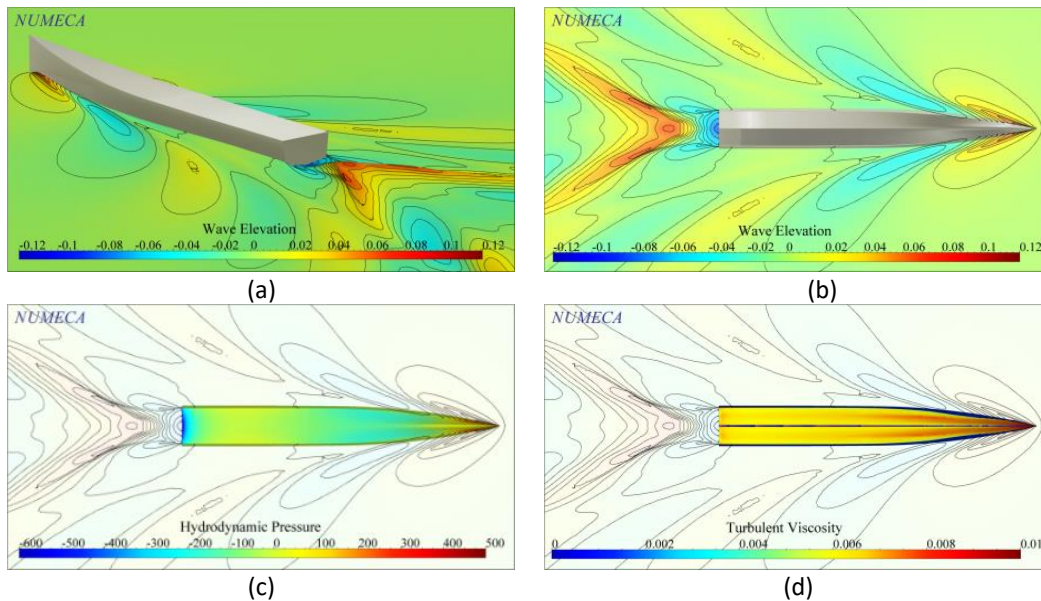
Fig. 4. Visualization on Axe-Bow Ship at Fr = 0.3946; (a) 3D Wave-Elevation, (b) 2D Wave-Elevation, (c) Hydrodynamic Pressure, (d) Turbulent Viscosity

3.1 Effect of Froude Numbers (Fr)

The resistance characteristics of the axe-bow ship at the various Froude numbers are displayed in Figure 5 to Figure 7. The total ship's resistance (R_T) is proportional to the subsequent increase of the forward velocities. It should be noted that the increment percentage of R_T tends to reduce from 17% to 11% when Vs increases from 2.487 m/s to 2.753 m/s and 4.412 m/s to 4.689 m/s, respectively. This can be explained by the fact that the total ship's resistance coefficient (C_T) has gradually decreased as Fr increases, see Figure 5(b). In addition, the results of the pressure (R_P) and viscous ship's resistances (R_V) are quite qualitatively similar to the trend of the total ship's resistance. Here, the increment percentage of the pressure ship's resistance is about 12% to 7% for the aforementioned changes of the forward velocities. Regardless of the forward velocities, it is interesting to note that the viscous ship's resistance has more relatively significant influence on the axe-bow ship than the pressure ship's resistance. The results indicate clearly that R_V increases by 20% and 13% on the stated similar forward velocities. The characteristics of the pressure and viscous ship's resistances and the corresponding details are as summarized in Table 4. Referring to Figure 6(b), so, it can be concluded that the axe-bow ship model has proven ability to satisfactorily reduce the pressure ship's resistance with respect to the increase of the forward velocities as similar trend to what was reported by Mosaad *et al.,* [2]. Meanwhile, the viscous ship's resistance becomes more dominant factor contributing to the total ship's resistance especially in the intermediate Froude number (Fr≥0.568) as displayed in Figure 7(b).
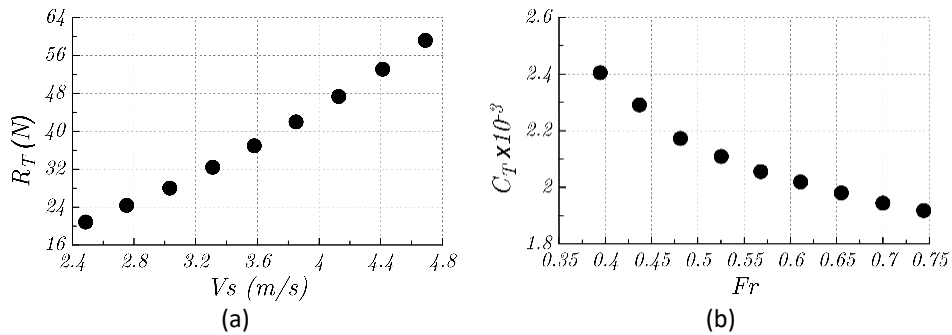
Fig. 5. (a) Total Resistance and (b) Resistance Coefficient of Axe-Bow Ship at Various Froude Numbers
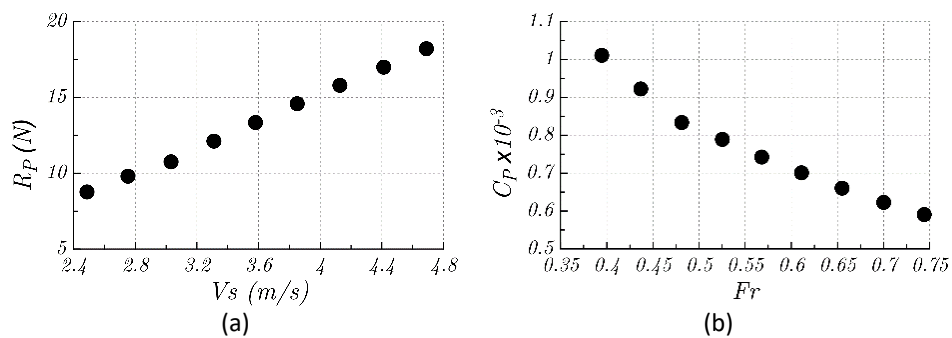
Fig. 6. (a) Pressure Resistance and (b) Pressure Coefficient of Axe-Bow Ship at Various Froude Numbers
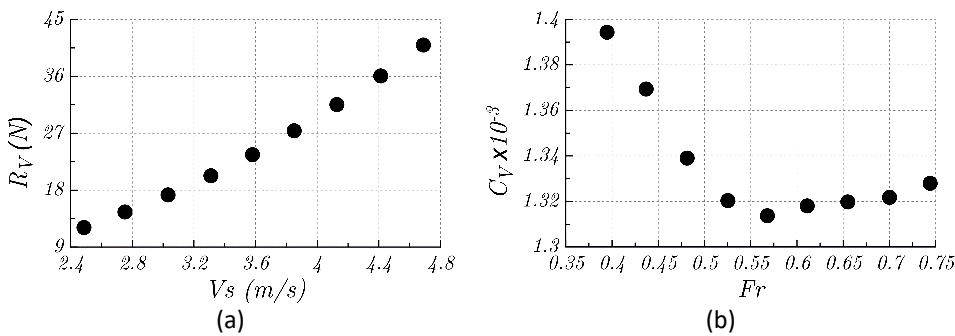
Fig. 7. (a) Viscous Resistance and (b) Viscous Coefficient of Axe-Bow Ship at Various Froude Numbers

Table 4
Resistance Characteristics of Axe-Bow Ship at Various Froude No.

V_s (ms^{-1})	F_r	R_T (N)	C_T (x10^{-2})	R_P (N)	C_P (x10^{-2})	R_V (N)	C_V (x10^{-2})
2.487	0.395	20.857	0.240	8.763	0.101	12.094	0.139
2.753	0.437	24.349	0.229	9.796	0.092	14.553	0.137
3.032	0.481	28.009	0.217	10.746	0.083	17.263	0.134
3.310	0.525	32.406	0.211	12.120	0.079	20.286	0.132
3.580	0.568	36.943	0.206	13.335	0.074	23.608	0.131
3.851	0.611	41.983	0.202	14.576	0.070	27.408	0.132
4.128	0.655	47.323	0.198	15.784	0.066	31.539	0.132
4.412	0.700	53.072	0.194	16.996	0.062	36.076	0.132
4.689	0.744	59.153	0.192	18.207	0.059	40.946	0.133

The characteristics of wave elevation, hydrodynamic pressure, and turbulent viscosity of the axe-bow ship at various Froude numbers have been displayed in Figure 8 to Figure 10. The increase of the total ship's resistance on the axe-bow ship is proportional with the magnitude of the wave elevation along the hull as shown in Figure 8(a) to Figure 8(h). As the subsequent increase of the forward velocities, inherently, this phenomenon leads towards producing the high-pressure gradients (red colour) that appear at the ship's bow regions as seen in Figure 9(a) to Figure 9(h). This could be also the basic reason of the augmented hydrodynamic pressure induced by the wave-making resistance particularly at the bow ship's region. It is noteworthy that the offset area of the wave-elevation nearby her bow's region becomes smaller (see Figure 8(i)) as the Froude number increase by 0.744; and causes C_P decrease indicated with moderately diminished high-pressures acting on the axe-bow ship's hull as displayed in Figure 9(i).
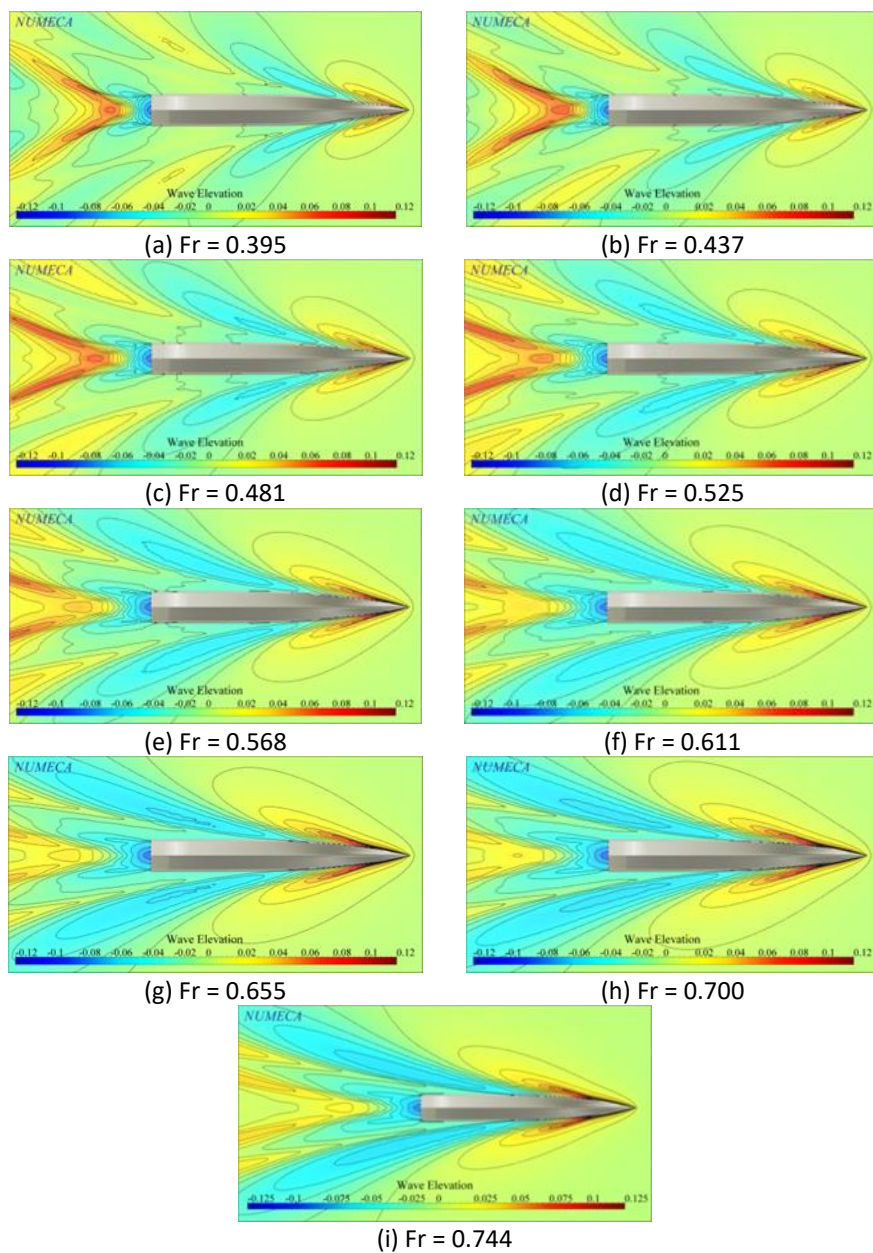
(a) Fr = 0.395

(b) Fr = 0.437

(c) Fr = 0.481

(d) Fr = 0.525

(e) Fr = 0.568

(f) Fr = 0.611

(g) Fr = 0.655

(h) Fr = 0.700

(i) Fr = 0.744

Fig. 8. Characteristics of Wave Elevation of Axe-Bow Ship at Various Froude Numbers

(a) Fr = 0.395   (b) Fr = 0.437

(c) Fr = 0.481   (d) Fr = 0.525

(e) Fr = 0.568   (f) Fr = 0.611

(g) Fr = 0.655   (h) Fr = 0.700

(i) Fr = 0.744
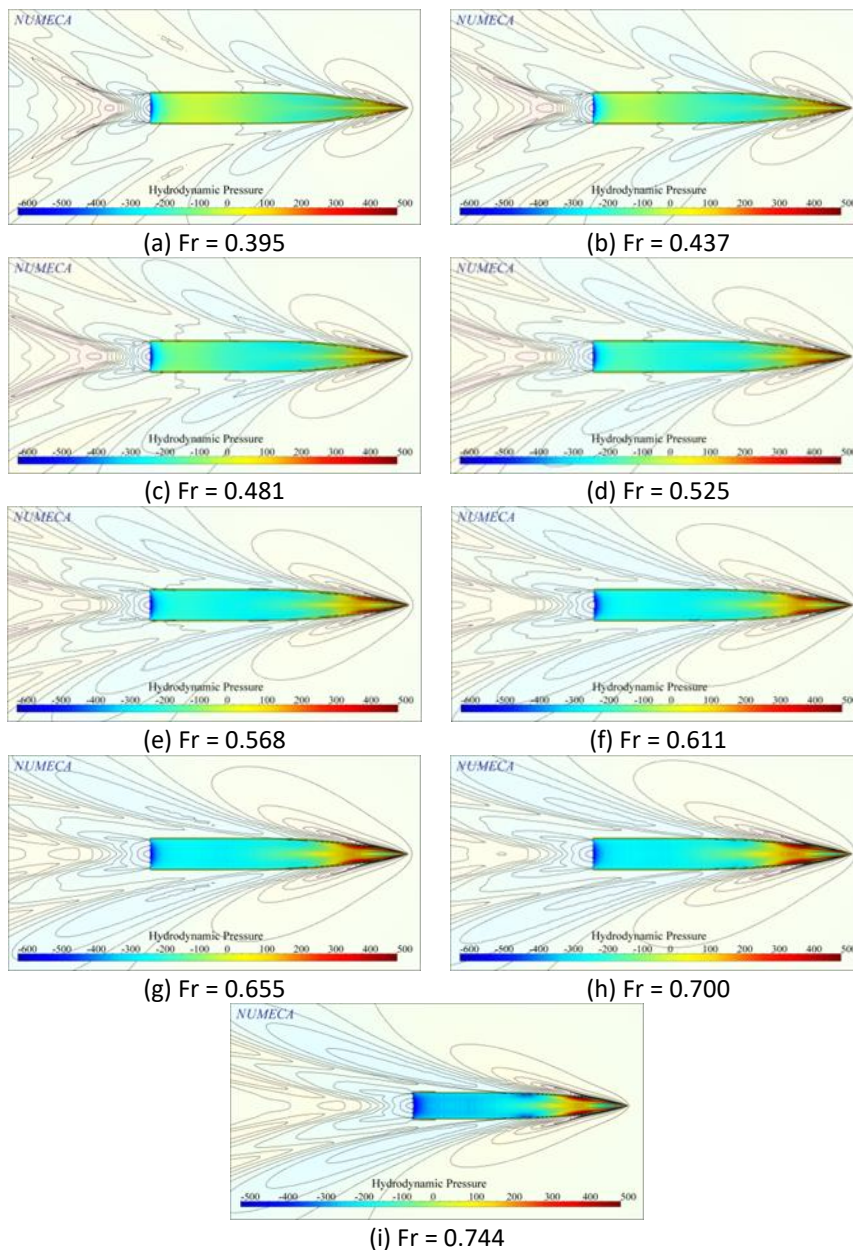
Fig. 9. Characteristics of Hydrodynamic Pressure of Axe-Bow Ship at Various Froude Numbers

Furthermore, the existence of the turbulent viscosity (yellow colour) at low speed extends over the entire hull surfaces of the axe-bow ship as displayed in Figure 10(a) to Figure 10(i). The CFD visualisation shows that the increase of the turbulent viscosity due to presence of more obvious red colour up Fr=0.7 causes the viscous resistance's coefficient reduces especially at the low-Froude number conditions (0.395≤Fr≤0.568). Furthermore, the red colour is moderately diminished, which results in C_V relatively increases within the range of intermediate Froude number (0.611≤Fr≤0.744). Referring to this finding, it is merely concluded that the viscous resistance of the axe-bow ship has relatively more influence into the total ship's resistance in the intermediate Froude number conditions instead of the pressure resistance.

(a) Fr = 0.395 (b) Fr= 0.437
(c) Fr = 0.481 (d) Fr = 0.525
(e) Fr = 0.568 (f) Fr = 0.611
(g) Fr = 0.655 (h) Fr = 0.700
(i) Fr = 0.744
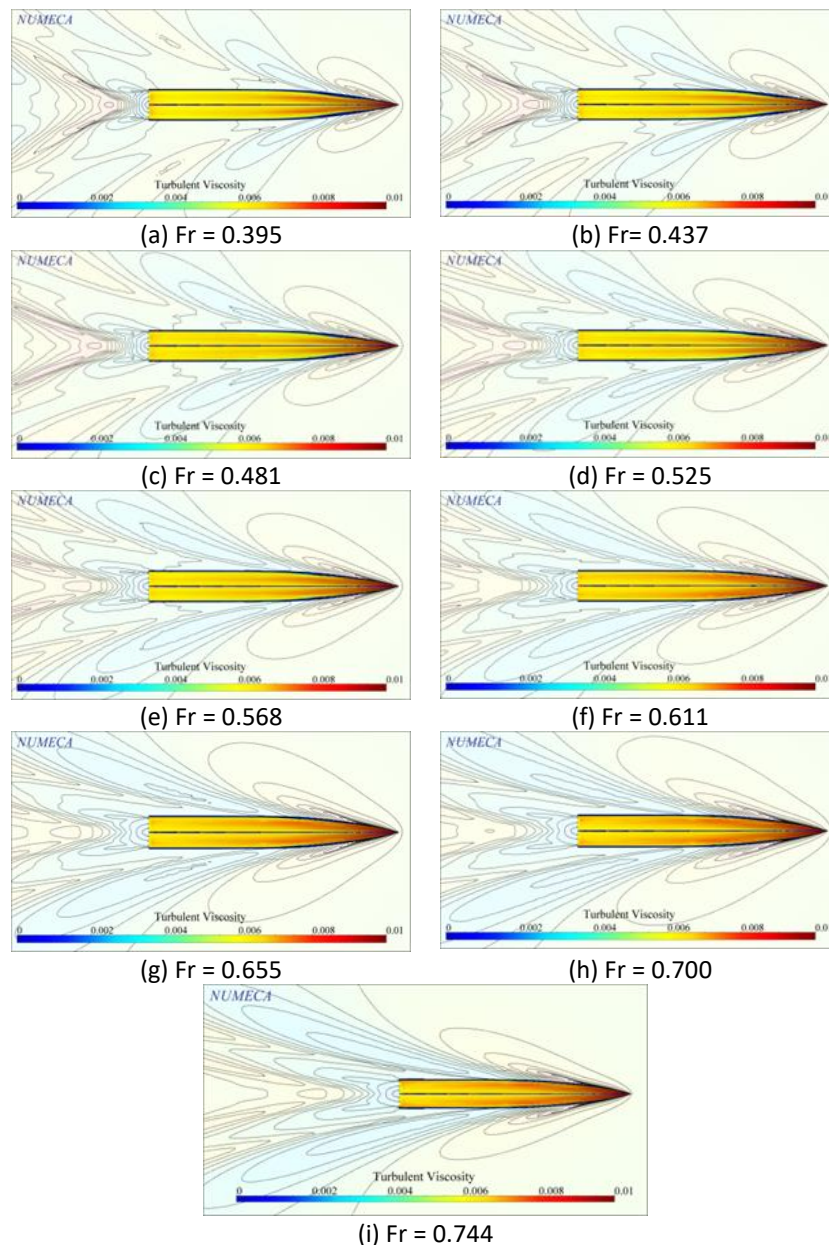
Fig. 10. Characteristics of Turbulent Viscosity of Axe-Bow Ship at Various Froude Numbers

3.2 Effect of Trim's Angle (α)

The computational investigation on the influence of the trim's angle in affecting the total ship's resistance of the axe-bow ship. Basically, this provides insight into a better understanding of her hydrodynamic characteristics via quantifying the pressure and viscous resistances. In general, the total ship's resistance is proportional with the increase of the trim's angles as displayed in Figure 11 to Figure 13. The results reveal that R_T increases by 11% and 13%; while R_P markedly increases by 33% and 42% as the ensuing trim by stern of the axe-bow ship from 0° to 1° and 1° to 2°, respectively. However, the effect of the aforementioned trim's angles is almost negligible on magnitude of R_V by 1% and 4%, respectively (negative means reduction). The detailed data of the pressure and viscous resistances of the axe-bow ship are completely presented in Table 5. Comparing the results of the axe-bow ship at the various trim's angle, in general, these are considered to have a moderately effect

corresponds to R_T and R_P increases by 7% and 13%, respectively. This seems reasonable finding, which can be comprehensively explained by pointing out the hydrodynamic characteristics.
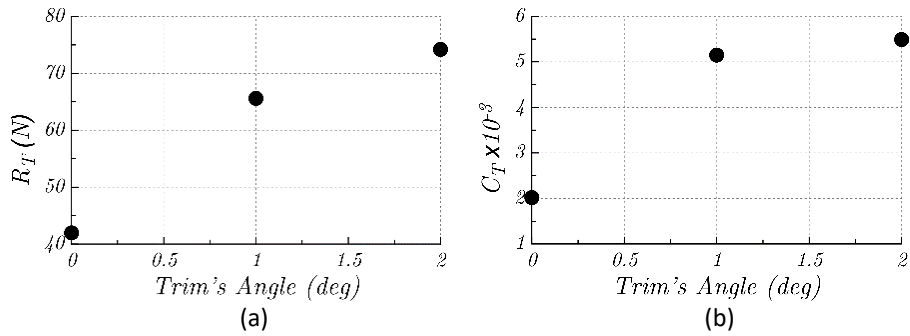
Fig. 11. (a) Total Resistance and (b) Resistance Coefficient (Right) of Axe-Bow Ship at different Trim's Angle
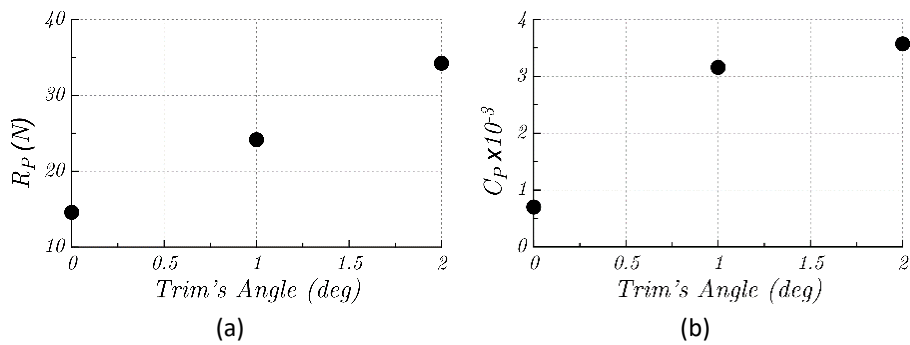
Fig. 12. (a) Pressure Resistance and (b) Pressure Coefficient of Axe-Bow Ship at different Trim's Angle (Fr = 0.744)
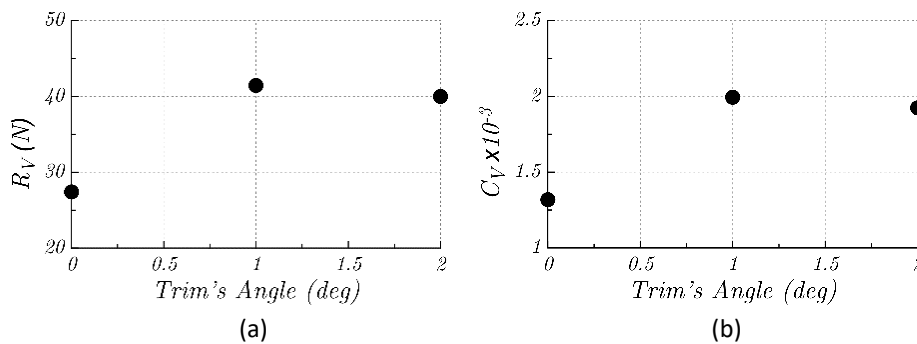
Fig. 13. Viscous Resistance (Left) and Viscous Coefficient (Right) of Axe-Bow Ship at different Trim's Angle (Fr = 0.744)

Table 5

Resistance Characteristics of Axe-Bow Ship at Various Trim's Angle (Fr = 0.744)

α (°)	R_T (N)	C_T (x10^{-2})	R_P (N)	C_P (x10^{-2})	R_V (N)	C_V (x10^{-2})
0	59.153	0.192	18.207	0.059	40.946	0.133
1	65.595	0.515	24.156	0.315	41.438	0.199
2	74.214	0.549	34.227	0.357	39.987	0.192

The investigation on the influence of trim's angle in affecting the ship's resistance of the axe-bow ship can be put forward through CFD visualization of the hydrodynamic behaviour along the ship's hull as depicted in Figure 14 to Figure 16. The total ship's resistance is proportional to the trim's angle. This can be explained by the fact that the subsequent increase of R_T occurs due to presence of

the high-pressure gradients at the bow's region (red colour). Yet, the hydrodynamic pressure notably disappeared especially when α increases from 1° to 2° as well as the significant reduction of the wave elevations, see Figure 14(c). It should be noted the pressure resistance sufficiently arises, which occurs due to more submerged part of the axe-bow ship hull. Correspondingly, this hydrodynamic pressure moves along the stern of the ship. At the same time, the suction regions reduce and converts slowly to the higher pressure, which consequently causes the higher wave-elevation. In addition, the characteristics of the turbulent viscosity acting on the hull surface is fully nonlinear phenomenon as the trim's angle increases from 1° to 2°. This demonstrates that the existence of the higher turbulent viscosity (yellow-red colour) extends over the entire submerged hull surfaces of the axe-bow ship as seen in Figure 16(b). However, the turbulent viscosity increases and imposes nearby her hull surfaces as displayed in Figure 16(c), which inherently gradually reduces C_V. Merely, this can be concluded that the increase of the pressure resistance coefficient has taken place dominantly; inversely, the viscous resistance coefficient reduces.

(a) 0°

(b) 1°

(c) 2°
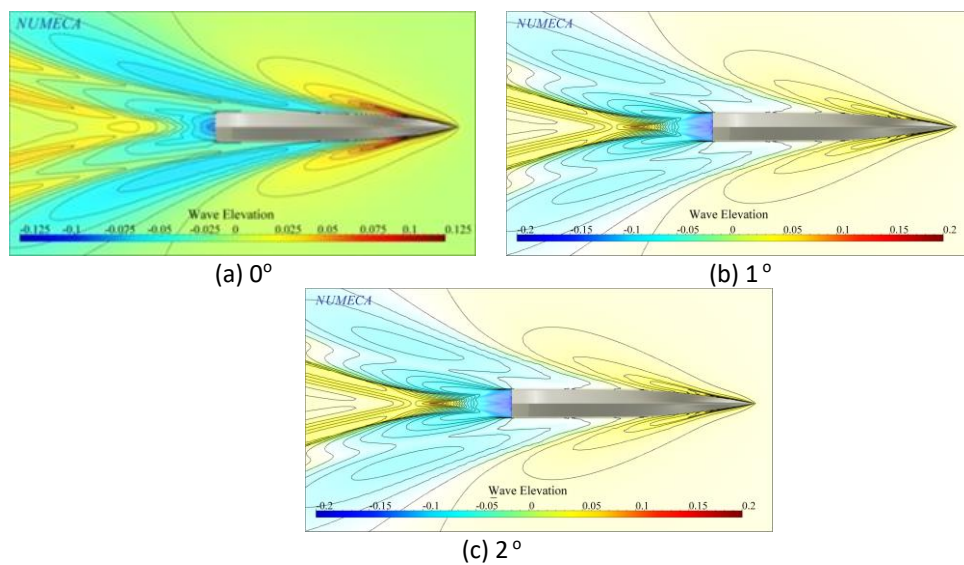
Fig. 14. Characteristics of Wave Elevation of Axe-Bow Ship at different Trim's Angle (Fr = 0.744)

(a) 0°

(b) 1°

(c) 2°
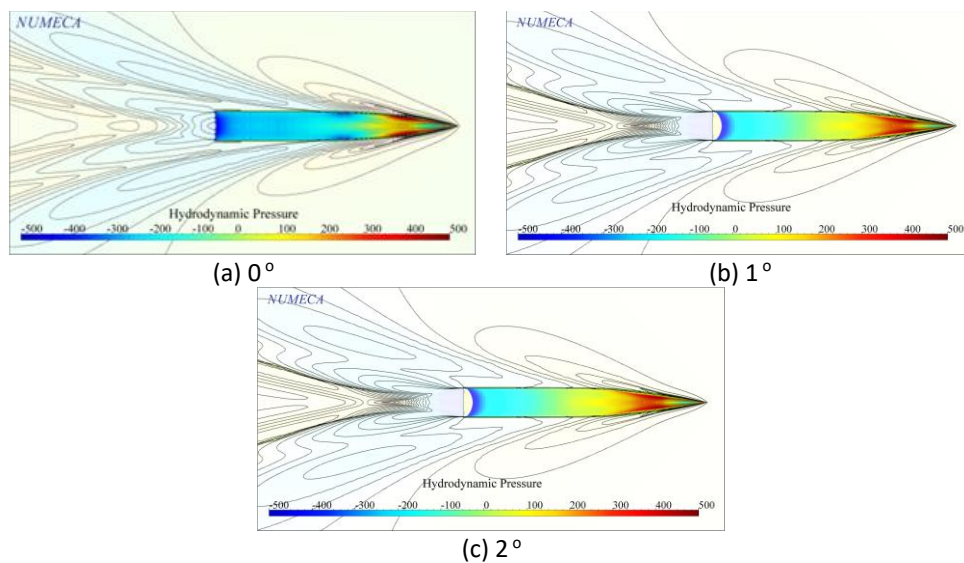
Fig. 15. Characteristics of Hydrodynamic Pressure of Axe-Bow Ship at different Trim's Angle (Fr = 0.744)

(a) 0°

(b) 1°

(c) 2°
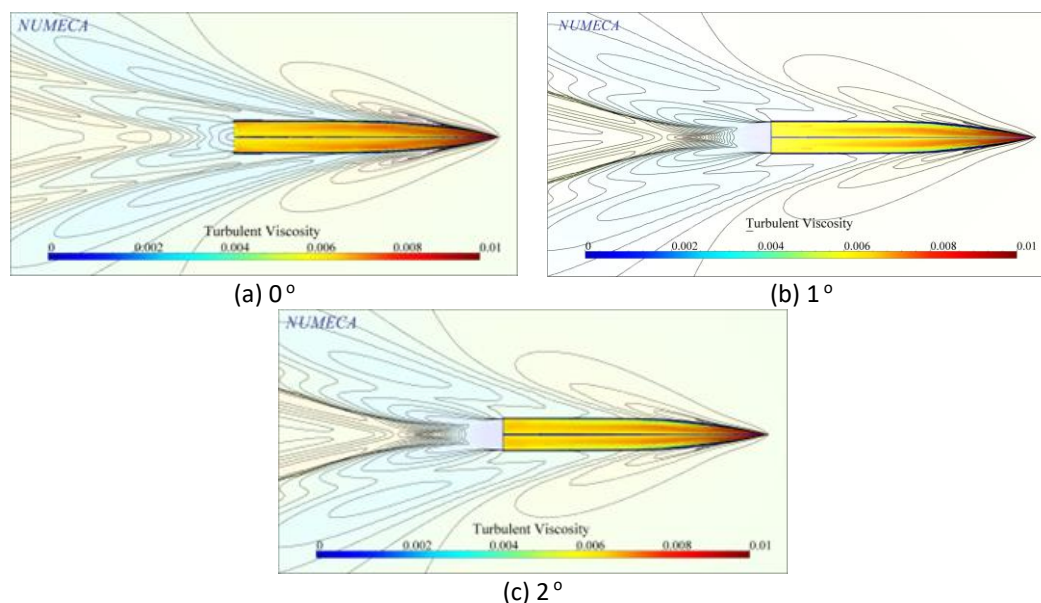
Fig. 16. Characteristics of Turbulent Viscosity of Axe-bow Ship at different Trim's Angle (Fr = 0.744)

4. Conclusions

Computational investigation into prediction the total ship's resistance on the axe-bow ship in the calm water condition is successfully performed. The effect of various Froude numbers and different trim's angle have been taken into account in the computational simulation. The results can be drawn as follows:

(a) The further increase of the Froude number by 0.744 causes C_P decreases indicated with moderately diminished high-pressures acting on the axe-bow ship's hull.

(b) Due to the increase of trim's angle increases from 1° to 2°, the pressure resistance coefficient has taken place dominantly; inversely, the viscous resistance coefficient reduces.

(c) In general, the subsequent increase of Froude number and the trim's angle are proportionally to the total ship's resistance.

References
[1] Hadi, E. S., and A. Firdhaus. "Total resistance analysis on bow form model ulstein X-bow with various angle of flare and stem angle." In *IOP Conference Series: Materials Science and Engineering*, vol. 674, no. 1, p. 012003. IOP Publishing, 2019. https://doi.org/10.1088/1757-899X/674/1/012003

[2] Mosaad, Mohamed A., M. M. Gafaary, Waleed Yehia, and Hussien Mohamed Hassan. "On the Design of Axe-bow for Ship Energy Efficiency." In *Influence of EEDI on Ship Design & Operation*, pp. 1-7. 2017.

[3] Basil, Kunjachan T., and Najdan Waris C. P. "Hull Optimisation of Fishing Trawlers Using Ulstein Axe-Bow And Bilge Keel." *International Journal of Engineering Applied Sciences and Technology* 7, no. 2 (2022): 214-220. https://doi.org/10.33564/IJEAST.2022.v07i02.032

[4] Simanjuntak, Frans, Samuel Samuel, Parlindungan Manik, Eko Sasmito Hadi, and Willma Amiruddin. "Analisis Pengaruh Pengunaan Ulstein X-Bow pada Kapal Perintis Type 750 DWT Terhadap Nilai Hambatan dengan Metode Computational Fluid Dynamics." *Rekayasa Hijau: Jurnal Teknologi Ramah Lingkungan* 5, no. 3 (2021): 248-266. https://doi.org/10.26760/jrh.v5i3.248-266

[5]   Chen, Shuling, Beilei Zou, Changzhi Han, and Shiqiang Yan. "Comparative Study on Added Resistance and Seakeeping Performance of X-Bow and Wave-Piercing Monohull in Regular Head Waves." *Journal of Marine Science and Engineering* 10, no. 6 (2022): 813. https://doi.org/10.3390/jmse10060813

[6]   Fitriadhy, A., and N. Amira Adam. "Heave and pitch motions performance of a monotricat ship in head-seas." *International Journal of Automotive and Mechanical Engineering* 14, no. 2 (2017): 4243-4258. https://doi.org/10.15282/ijame.14.2.2017.10.0339

[7]   Zikry, Syafiq, and Ahmad Fitriadhy. "Seakeeping performance of a hydrofoil in waves using cfd approach." *Universiti Malaysia Terengganu Journal of Undergraduate Research* 3, no. 3 (2021): 167-176. https://doi.org/10.46754/umtjur.2021.07.017

[8]   Rahman, Mustafizur, M. A. Alim, Suman Saha, and M. K. Chowdhury. "Mixed convection in a vented square cavity with a heat conducting horizontal solid circular cylinder." *Journal of Naval Architecture and Marine Engineering* 5, no. 2 (2008): 37-46. https://doi.org/10.3329/jname.v5i2.2504

[9]   Fitriadhy, Ahmad, Nur Adlina Aldin, and Nurul Aqilah Mansor. "CFD analysis on course stability of a towed ship incorporated with symmetrical bridle towline." *CFD Letters* 11, no. 12 (2019): 88-98.

[10]   Fitriadhy, Ahmad, and Amira Adam. "CFD analysis on vertical motion of a full-scale floating jetty." *Journal of Sustainability Science and Management* 15, no. 6 (2020): 100-110. https://doi.org/10.46754/jssm.2020.08.009

[11]   Fitriadhy, Ahmad, Nur Amira Adam, C. J. Quah, Jaswar Koto, and Faisal Mahmuddin. "CFD prediction of b-series propeller performance in open water." *CFD Letters* 12, no. 2 (2020): 58-68.

[12]   Fitriadhy, Ahmad, Intan Nur Nabila, Christina Bangi Grosnin, Faisal Mahmuddin, and Suandar Baso. "Computational Investigation into Prediction of Lift Force and Resistance of a Hydrofoil Ship." *CFD Letters* 14, no. 4 (2022): 51-66. https://doi.org/10.37934/cfdl.14.4.5166

[13]   Fitriadhy, Ahmad, Loke Yan Pheng, Iqmal Nor Hakim Adzkh, Faisal Mahmuddin, Anuar Abu Bakar, Mohd Azlan Musa, and Mohd Sofiyan Sulaiman. "Computational Investigation of Pitch Motion of a High-Speed Craft Incorporated with Trim-Tabs." *CFD Letters* 14, no. 6 (2022): 56-71. https://doi.org/10.37934/cfdl.14.6.5671

[14]   Mirzaei, Mahdi, A. Maimun, A. Priyanto, and A. Fitriadhy. "Mooring pattern optimization using a genetic algorithm." *Jurnal Teknologi* 66, no. 2 (2014): 189-193. https://doi.org/10.11113/jt.v66.2519

[15]   Menter, Florian, and Christopher Rumsey. "Assessment of two-equation turbulence models for transonic flows." In *Fluid Dynamics Conference*, p. 2343. 1994. https://doi.org/10.2514/6.1994-2343

[16]   Spalart, Philippe, and Steven Allmaras. "A one-equation turbulence model for aerodynamic flows." In *30th Aerospace Sciences Meeting and Exhibit*, p. 439. 1992. https://doi.org/10.2514/6.1992-439

[17]   Molland, A. "Resistance experiments on a systematic series of high speed catamaran forms: Variation of length-displacement ratio and breadth-draught ratio." *Transactions of the Royal Institution of Naval Architects* 138 (1996): 59-71.